BIO Integration



# Experimental Study on the Viscoelastic Flow Mixing in Microfluidics

Meng Zhang[1,2,*], Wu Zhang[3,a,*], Zihuang Wang[3] and Weiqian Chen[3]


## Abstract

**Background:** The study of blood flow in vessels is always crucial to understand cardiovascular diseases such as arrhythmias, coronary artery disease and deep vein thrombosis. A viscoelastic fluid in a microchannel is modeled for the blood flow study.

**Methods:** In this paper, we modeled the blood flow through a viscoelastic fluid in a microfluidic channel. The flow properties, especially the flow pattern and transient mixing of two fluid streams in a T-shaped microchannel, are experimentally studied.

**Results:** It was found that the viscoelastic fluid has a transiently unstable flow pattern compared to the normal Newtonian fluid, and the mixing is also increased due to its elastic property. Similar to the pulsatile blood flow, the fluid is driven under a periodically pulsed stimulus, and the flow pattern and transient mixing are compared at different flow rates and driving period conditions.

**Conclusions:** The integration of microfluidic technology with the blood flow research could provide a new approach to understand the related disease mechanism, which can also be used to analyze the drug mixing and delivery in the blood flow.



## Keywords

Microfluidics, viscoelastic flow, mixing.



[1]The First Affiliated Hospital of Sun Yat-Sen University, Sun Yat-Sen University, Guangzhou 510080, China

[2]School of Engineering and Applied Science, Harvard University, Cambridge, MA 02138, USA

[3]School of Physics and Material Science, Guangzhou University, Guangzhou 510006 China

[a]Wu Zhang have contributed equally in this manuscript as the co-first author.
*Correspondence:
Meng Zhang
E-mail: meng.zhang_china@outlook.com
Wu Zhang
E-mail: zh0002wu@outlook.com



Received: August 3 2020
Revised: August 24 2020
Accepted: August 27 2020
Published Online: December 1 2020

Available at:
https://bio-integration.org/


## Introduction

Microfluidic technology uses micro-scaled channels, chambers and valves to control and manipulate single-phased or multi-phased fluids in the microliter to picoliter volume range, and deliver, mix or synthesize substances in the fluid. The fluid manipulation is confined to the micrometer-scaled space and therefore offers many advantages which has not been realized in traditional methods. It requires much less sample liquid, allows rapid diffusion and has a faster reaction in the micro-chambers to save time for testing or synthesizing. The designable microchannel structure also offers large freedom to control the liquid flow. Since its emergence, microfluidic technology has attracted much research attention in different areas including fluid dynamics, nanotechnology, biochemistry, biotechnology and clinical applications. The integration of microfluidic technology with biotechnology and clinical research has promoted a lot of applications in tissue engineering [1, 2], disease diagnosis [3, 4] and gene delivery and transfer [5]; some examples are listed in **Table 1**.

Among the aforementioned biotechnology and clinical applications, the mixing of substances in the microfluidics is one important process. In the microfluidic mixer, the synthesis and delivery of lipid or drug-loaded nanoparticles [6, 7] or microgels [8] are realized. For example, lipid nanoparticles containing small interfering RNA (siRNA) are synthesized by microfluidic mixing for enabling therapeutic applications [9]. The nanoparticles are also used for lipofection of plasmid DNA into human mast cell lines [10]. In addition, the microfluidic mixer promotes the biosensing applications. An active mixing method was proposed to increase the capture efficiency in a heterogeneous microfluidic immunosensor [11]. A micro-mixing system was later developed for the detection of immunoagglutination [12] and rapid labeling of immune cells with antibodies [13]. Simultaneous genetic detection of multiple plant viruses was also realized through an autonomous microfluidic sample mixing device [14]. More importantly, the microfluidic mixing technology has already manifested great potential in diagnosis and therapy applications. A microfluidic device was developed to tunably mix reactive oxygen species for optimizing photodynamic therapy [15]. The control of drug release was also realized


https://bio-integration.org doi: 10.15212/bioi-2020-0029

**Table 1** Integration of Microfluidic Technology with Biotechnology and Clinical Research

| Bio-applications | Different Categories | Specific Applications and References |
|---|---|---|
| Tissue engineering | Microfluidic scaffolds | Simulate native tissue microstructures for drug delivery control [1]<br>Study cancer cell migration in controlled microenvironments [25] |
| | Microfluidic cell culture | Automatic culturing cells with no manual interference [26]<br>Quantifying cell response in co-culture architectures [2] |
| Disease diagnosis | Isolation of circulation tumor cells | Optical dielectrophoresis microfluidic system for cell isolation [27]<br>Surface antigen bonding method in microfluidic channels [3]<br>Vortex chip for high-throughput and label-free cell purification [28] |
| | Biomarker detection | One-step multiplexed pathogen detection with nano-biosensors [4]<br>Microfluidic droplets as bioreactors for enzymatic amplification [29] |
| Gene delivery and therapy | Gene transfection | Deliver genes into cells in microfluidic electroporation systems [30]<br>Generate inertial vortex to enhance gene transfection efficiency [31] |
| | Production of gene carriers | Microfluidic system to improve the production of retroviral vectors [5]<br>Biosynthesis reactor for synthesizing DNA-polycation complex [32] |

through stabilized polymeric nanoparticles generated in an efficient microfluidic mixing system [16]. A passive mixing microfluidic urinary albumin chip was later demonstrated for chronic kidney disease assessment [17].

In the aforementioned works, a conventional Newtonian fluid is usually used as the fluid carrier in microfluidic mixing devices. However, most body fluids, especially blood, have different hydrodynamic properties with conventional Newtonian fluids. Such liquids process both viscosity and elasticity, and are categorized as viscoelastic fluids. The viscoelastic fluid plays an important role in the circulation system of the human body; the study of its flow properties will greatly help to understand the human physiology. The flow of blood in vessels has been widely studied in both theoretical and experimental aspects [18–21]. In one study, Chakravarty and Mandal investigated the blood flow in overlapping stenosed vessels, the wall of which is assumed to be elastic and deformable [22]. The blood flow through the overlapping stenosed vessels was also numerically and analytically studied by Riahi et al. [23]. The fluid in the aforementioned model is assumed to be Newtonian; however, in a realistic situation, the blood flow in vessels is viscoelastic. Therefore, fluid models with both viscosity and elasticity are proposed to study these flows. Different non-Newtonian characteristics such as yield stress, pseudo-plasticity and viscoelasticity [24] are investigated at different shear rates.

The mixing of viscoelastic fluid in the microfluidic system was also intensively studied and found to be much larger than that of the Newtonian fluid [33]. The enhanced mixing is usually achieved by generating vortex in the viscoelastic microfluidic flow due to the elastic stress in the fluid, which is not observed in the Newtonian flow even at high flow rate conditions [34–36]. An early experiment found a significant difference between Newtonian and non-Newtonian fluids, and concluded that the shear thinning behavior of the blood could be the dominant non-Newtonian property [37]. On the other hand, a work discusses the importance of extensional rheology, in addition to the shear rheology of solutions when mimicking the blood circulation system [38]. New technologies such as the micro-particle image velocimetry (PIV) technique were then applied to analyze the human blood flow [39]. A recent study investigated the unidirectional large-amplitude oscillatory shear flow of the blood to assess its non-Newtonian behaviors, which describes well the unidirectional pulsatile flow in veins and arteries [40]. Here, we studied the viscoelastic flow in a T-shaped microchannel structure, which mimics the blood flow in the bifurcated vessels as shown in **Figure 1A**. Two streams of viscoelastic fluid are injected into a T-shaped microchannel and pumped with periodical pulse, mimicking the pulse of blood in vessels. Specifically, the flow pattern and mixing of the two streams are monitored transiently. The integration of microfluidic technology with the blood flow research could not only provide a new approach to understand the related disease mechanism, but also be used to analyze the drug mixing and delivery in the blood flow.

## Methods

In this paper, the polyacrylamide (PAM) solution is used as the viscoelastic fluid to mimic the blood flow in the microchannel structure. Here, we use the PAM solution of 200 ppm molecular weight. As shown in **Figure 1B**, the microchannel is a T-shaped structure, which is fabricated on a poly(dimethylsiloxane) (PDMS) layer through the typical soft lithography method. The PDMS layer is then bonded with a glass slide as shown in **Figure 1C**. In the experimental setup, the solution is injected into both inlet A and inlet B, which are noted as fluid A and fluid B with injection flow rates of $Q_A$ and $Q_B$, respectively. The flow rates are controlled by two flow pumps independently. After entering the microchannel, the two fluids first meet at the center of the "injection channel" and then pass through a narrow "bottleneck channel" before entering the abruptly expanded "mixing channel". To evaluate the mixing effect between the two pumped fluids, the fluorescent dye rhodamine B is pre-mixed with fluid A. Rhodamine B can be excited by a 435-nm-wavelength laser and radiate fluorescent light. The fluorescence intensity of the fluid changes as the two fluids mix with each other in the microchannel, and can thus be used to assess the mixing degree in the microchannel.

The fluorescent light intensity is recorded as a gray value at each pixel point in the mixing channel for a long enough time, and the fluid mixing degree is analyzed according to the gray values. In this experiment, the flow patterns are

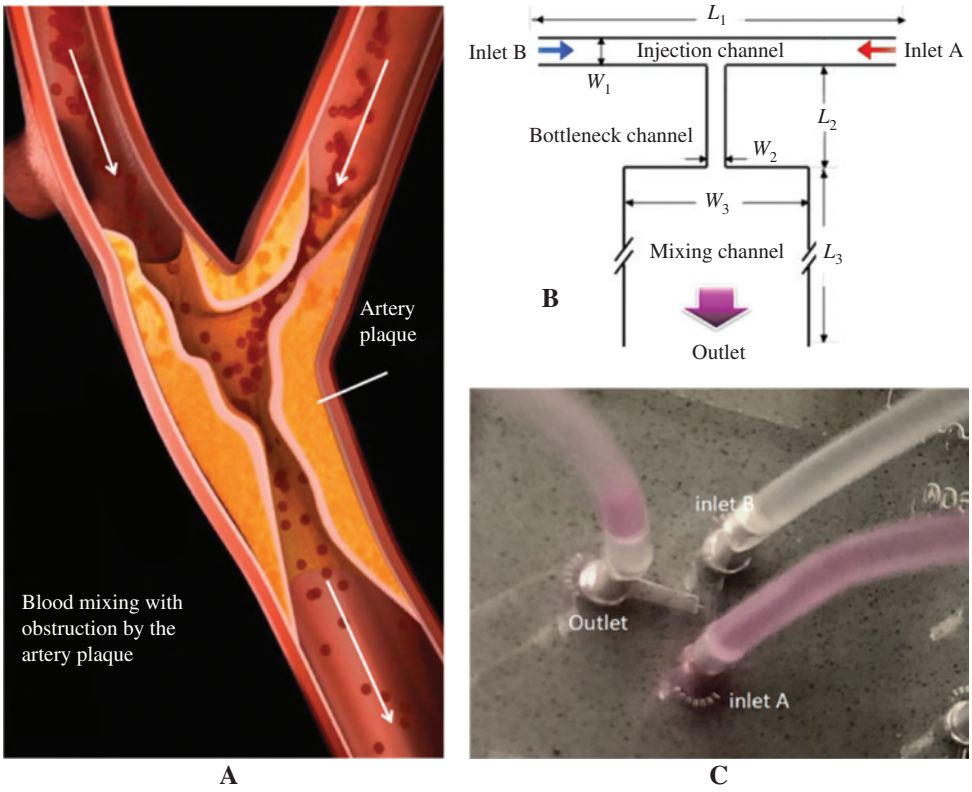


**Figure 1** (A) A schematic of the blood flow in veins, (B) a schematic of a T-microchannel for mimicking the blood flow in veins and (C) the PDMS-glass chip for the T-microchannel.

recorded by a high-speed camera with 2048 pixels × 2048 pixels, and the resolution of each pixel is 0.769 μm.

The relaxation time and shear rate of the PAM solution used here are 100/s and 0.12 s, respectively. The concentration of rhodamine B fluorescent dye in fluid A is 10 μg/mL. At such a low concentration, its effect on mixing can be ignored. The size of the T-shaped microchannel is as follows: the length and width of the "injection channel", "bottleneck channel" and "mixing channel" are $L_1$ = 2 mm, $W_1$ = 100 μm, $L_2$ = 600 μm, $W_2$ = 50 μm, $L_3$ = 2 mm and $W_3$ = 600 μm, respectively. The end of the "mixing channel" is connected to the microchannel outlet. In the T-shaped design, the channel design is symmetrical to simplify the analysis. The mixing is further enhanced by an abrupt expansion of the microchannel with $W_3$ = 12 $W_2$. In the experimental records, the microscope focused at the central plane of the flow.

# Experimental results and discussion

## Mixing in the constant injection condition

Before the study of the viscoelastic fluid mixing in the microchannel, we first investigated the mixing of a Newtonian fluid. The glycerol solution is injected into inlet A and inlet B and the corresponding flow rates $Q_A$ and $Q_B$ are first controlled at a same constant value $Q_0$. **Figure 2A** presents the contour map of the fluorescent dye concentration when $Q_0$ = 100 μL/h. The color bar represents the normalized dye fluorescent intensity with an arbitrary unit. The red region at the fluid A side stands for concentration 1, and the blue region at the fluid B side stands for concentration 0. The two fluids flow through the bottleneck channel and enter into the mixing channel. The dye concentration profile is stable and a smooth boundary region (green color) is observed in between, which is due to the diffusion of the fluorescent dye during the mixing between fluid A and fluid B. When the injected flow rate increases from 100 μL/h to 500 μL/h as shown in **Figure 2B**, the diffusion effect decreases and the mixing region shrinks. While for the viscoelastic PAM solution, the mixing is much different from that of the glycerol solution as shown in **Figure 2C** and **2D**. When the PAM solution is injected into the microchannel at $Q_0$ = 100 μL/h, the mixing region is significantly larger than that in the glycerol solution. The florescence concentration decreases at the fluid A side and increases at the fluid B side compared to the glycerol solution mixing case, indicating an enhanced mixing of the two fluids. PAM has the same viscosity as glycerol; therefore, the mixing increase must stem from the non-zero elasticity in PAM. The elasticity of PAM arises from the interaction between its molecular structure and the flow. The flow conditions induce force on the polymers in the fluid and the polymer chains are stretched and oriented. This non-equilibrium configuration imposes large anisotropic normal stresses, which themselves influence the flow field and the mixing effect, and also explain the relatively rough boundary between the two side fluids. As $Q_0$ increases to 500 μL/h, the elastic interaction between the two

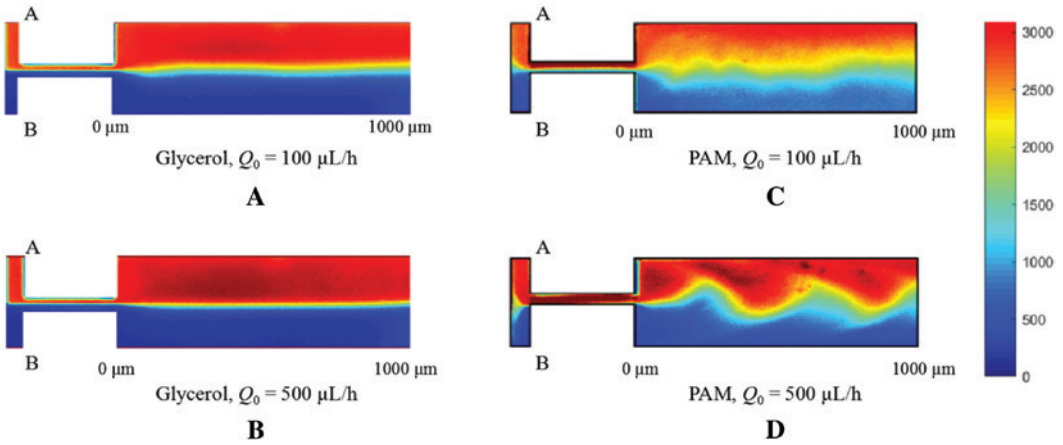


**Figure 2** Concentration profiles of (A) glycerol at $Q_0$ = 100 μL/h, (B) glycerol at $Q_0$ = 500 μL/h, (C) PAM at $Q_0$ = 100 μL/h and (d) PAM glycerol at $Q_0$ = 500 μL/h.

side fluids is further enhanced and a "wave" shaped boundary is observed. The "wave" shape propagates forward in the microchannel and therefore the fluorescent dye distribution at one specific cross-section keeps changing. This special boundary is due to the stronger elastic force between the two fluids. Now the dye concentration profile keeps changing as the "wave" shaped boundary moves forward. The mixing region becomes smaller than that when $Q_0$ = 100 μL/h; the decreased mixing efficiency is due to the lowered diffusion at the higher flow rate condition.

## Mixing in the periodically pulsed injection condition

To mimic the pulsatile blood flow in veins and arteries, the injected flow rate of fluid A is pulsed with a square wave signal, while the flow rate of fluid B remains at a constant value, which can be expressed as:

$$Q_A(t) = Q_0\{1 + sgn[sin(2\pi ft)]\} \quad (1a)$$

$$Q_B = Q_0 \quad (1b)$$

where $f$ is the modulated frequency on fluid A and $t$ is the flow time. The modulation of the driving stimulus can better integrate the microfluidic technology with the real blood flow study. The flow patterns of the viscoelastic solution in the microchannel at different modulated frequencies with $Q_0$ = 100 μL/h and $Q_0$ = 500 μL/h are illustrated in **Figure 3A** and **3B**. At $Q_0$ = 100 μL/h, the distribution of the fluorescence in the microchannel remains almost unchanged as the modulation frequency $f$ varies. In addition, when $f$ = 0.1 Hz (T = 10 s), a small "wave" shaped boundary can be observed between fluid A and fluid B when the fluids flow into the mixing channel. This is because at this lower frequency, more fluid A and fluid B enter the mixing channel in one period and interact with each other elastically. At the relatively high flow rate of 500 μL/h, the fluorescence concentration distribution in the fluid showed a distinct "wave" shape at the boundary between fluid A and fluid B at different modulation frequencies including $f$ = 0. The spatial "wave" period is equal to about 665 μm at different modulated frequencies, which is determined by the elasticity of the viscoelastic fluid itself. It can be observed that with the frequency modulation, the concentration of the fluorescent dye distributes differently.

As the driving signal varies periodically in time, the flow in the microchannel and the mixing degree of fluid A and fluid B also change periodically. The transient mixing degree

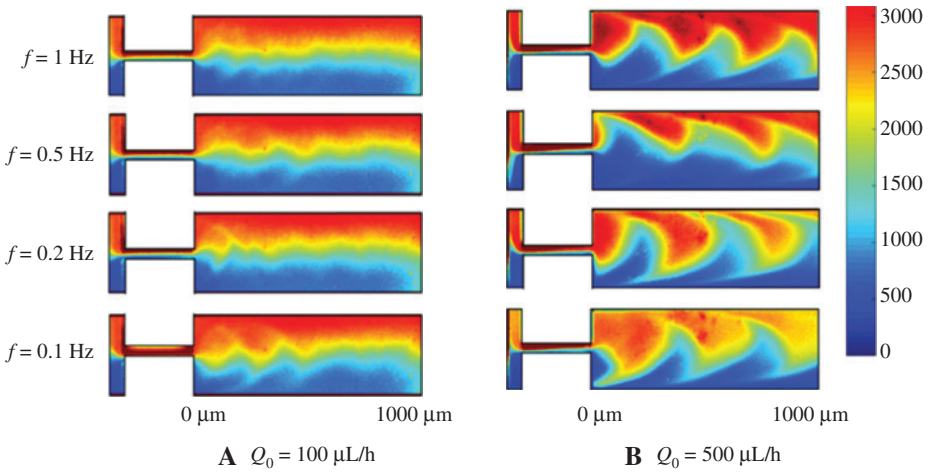


**Figure 3** Mixing map of the PAM solution at different modulation frequencies when (A) $Q_0$ = 100 μL/h and (B) $Q_0$ = 500 μL/h.

$MD_t$ is calculated to quantitatively analyze the mixing efficiency. On the cross-line at the flow distance $S_0$ after entering the mixing channel, the transient mixing degree at time $t$ is expressed as:

$$MD_t = 1 - \sqrt{\sum_{i=1}^{P} \frac{\left(\frac{C_i}{C_0} - 1\right)^2}{P}} \quad (2)$$

In equation (2), $C_i$ is the gray value of pixel $i$ on the $S_0$ cross line at time $t$ when the video is recorded under the microscope. There are a total of $P$ pixels on the cross-line, and $C_0$ is the average gray value.

We investigated the transient mixing degree of both glycerol solution and PAM solution as shown in **Figures 4** and **5**, respectively. The x-axis in the figures represents the monitored flowing distance, starting at 0 when entering the "mixed channel", and the flow with a total distance of 1000 μm is recorded. The y-axis is the recorded time. The color map represents the transient mixing degree when fluid A is modulated by the above square wave signal at the (a) constant flow rate condition, (b) $f$ = 1 Hz, (c) $f$ = 0.2 Hz and (d) $f$ = 0.1 Hz periodically driving condition. The four contour maps in each sub-figure are the transient mixing degree when $Q_0$ = 100 μL/h, $Q_0$ = 200 μL/h, $Q_0$ = 500 μL/h, and $Q_0$ = 1000 μL/h, correspondingly.

In the glycerol solution fluid with a constant flow rate (**Figure 4A**) or when the driving frequency $f$ = 1 Hz (**Figure 4B**), the transient mixing degree was only around 10% for the most of the time at all tested flow rates from 100 μL/h to 1000 μL/h. As the modulation frequency varies to $f$ = 0.2 Hz (**Figure 4C**) and $f$ = 0.1 Hz (**Figure 4D**), the transient mixing degree remains at a low value when the flow rate $Q_0$ is at 100 μL/h and 200 μL/h condition. While at the $f$ = 0.2 Hz and $f$ = 0.1 Hz conditions with $Q_0$ = 500 μL/h and 1000 μL/h, it can be observed that a periodical high mixing degree of around 50% is obtained at the specific time when entering the mixing channel, the period of which equals to the modulating signal period. The increase in the transient mixing degree results from the unbalanced injection between fluid A and fluid B. At the lower modulation frequency and higher injection flow rate, the volume difference between the two fluids entering the microchannel is larger in every half cycle; therefore, there is a large unbalanced force between the two fluids. The direction of the force keeps changing as the injected flow rate of fluid A is modulated, which disturbs the flow and increases the mixing efficiency. The improvement in mixing recurs at every modulated period, and forms a periodical band in the contour map.

In contrast, as shown in **Figure 5**, the transient mixing degree of the PAM solution in the viscoelastic fluid is generally above 50% at different driving boundary conditions and injected flow rates, which is significantly higher than that of the Newtonian fluid glycerol solution. The increase in the mixing degree is caused by the elastic stress inside and mutual compression between fluid A and fluid B. For the constant flow rate injection case (**Figure 5A**) and $f$ = 1 Hz modulation condition (**Figure 5B**), a significant increase in the mixing degree is found at certain flow distance and flow time when the flow rate $Q_0$ increases to 1000 μL/h. This high mixing fluid region (the red color region) starts at the beginning of the mixing channel (flow distance = 0), and the mixing degree increases gradually as the fluid flows through the mixing channel. This is due to the elastic interaction between fluid A and fluid B, and the diffusion continues to contribute to the mixing effect. As the modulation frequency decreases to $f$ = 0.2 Hz and $f$ = 0.1 Hz, an obvious high mixing band can be observed at the high flow rate of $Q_0$ = 500 μL/h and $Q_0$ = 1000 μL/h, which changes periodically in time with period equaling to the modulation period. The increase in the mixing degree stems from the external driving force which periodically stretches and compresses the polymer inside fluid A

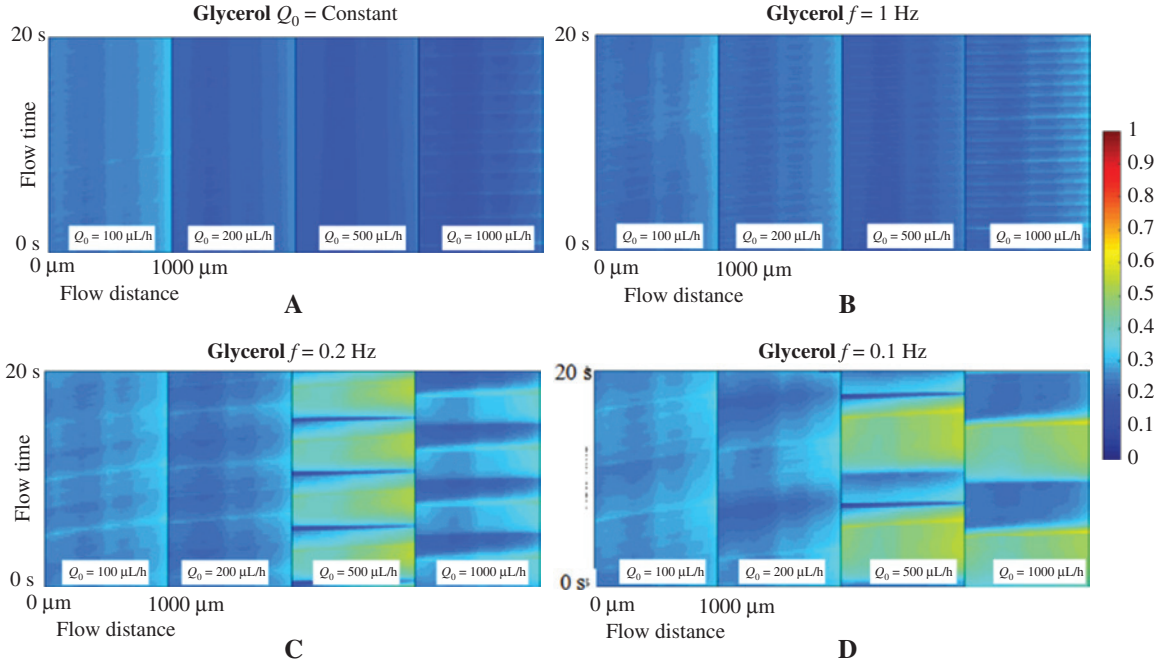


**Figure 4** Transient mixing degree of the glycerol solution at (A) a constant injection rate, (B) $f$ = 1 Hz, (C) $f$ = 0.2 Hz and (d) $f$ = 0.1 Hz.

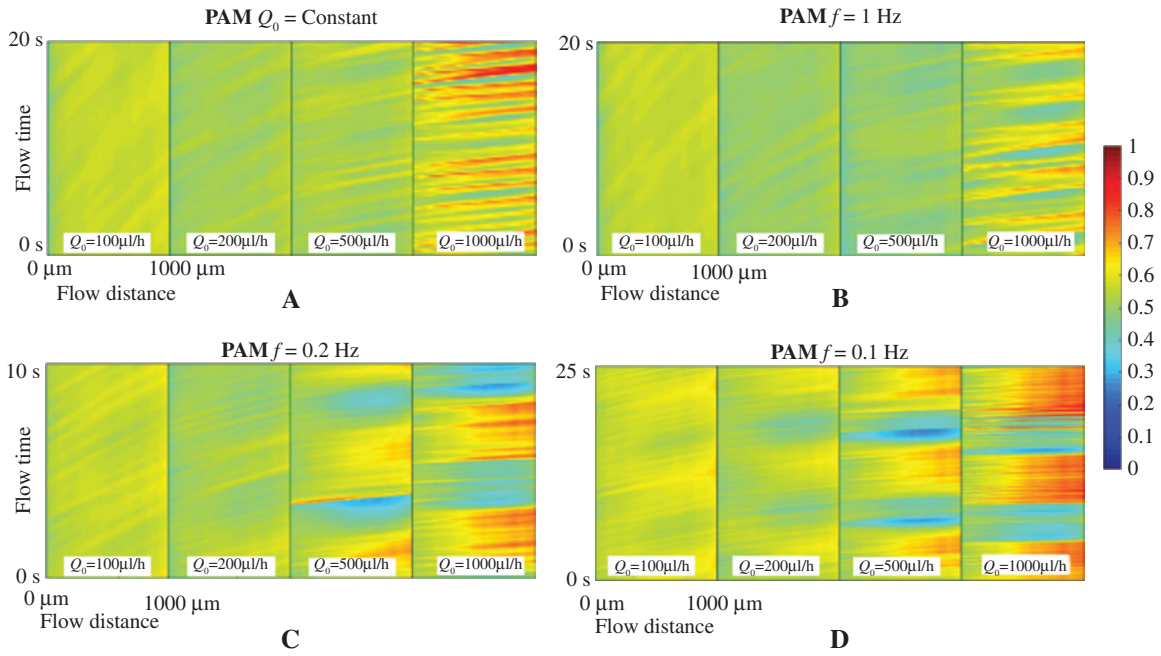


**Figure 5** Transient mixing degree of the PAM solution at (a) a constant injection rate, (b) $f$ =1 Hz, (c) $f$ = 0.2 Hz and (d) $f$ = 0.1 Hz.

and fluid B. This stretch and compression will drive the elastic interaction between the two fluids periodically and form a high mixing fluid part. This high mixing part flows through the mixing channel, in which fluid A and fluid B continue to mix with each other, and realize a high transient mixing degree above 70% at certain flow time and flow distance.

## Mixing in different geometric microchannels

The mixing is also studied in the T-shaped microchannel at different geometric parameters. We first increased the width of the mixing channel from 600 μm to 1400 μm as shown on the left side of **Figure 6A**. When the fluid enters the mixing channel from the bottleneck channel, it will form an extensional flow due to the expansion of the channel width. The extension of the flow will stretch the polymer in the viscoelastic fluid and therefore affect the mixing effect. As the width of the bottleneck channel is fixed at 50 μm, the expansion ratio increases from 12 to 28 in the new geometric structure. The transient mixing degrees of the fluid PAM solution at $Q_0$ = 500 μL/h are shown on the right side of **Figure 6A**. When the injected flow rate is constant or when the modulation frequency $f$ = 1 Hz, the fluctuation of the transient mixing degree is small compared with that when

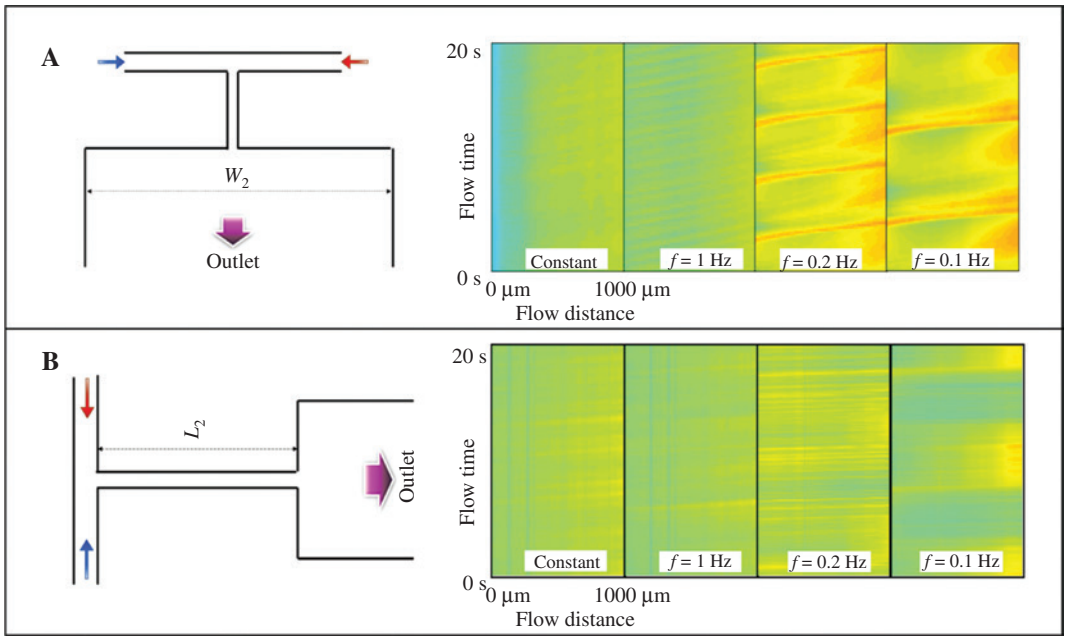


**Figure 6** (A) Schematic of a wide T-microchannel and the corresponding transient mixing degree of the viscoelastic fluid. (B) Schematic of a long bottleneck T-microchannel and the corresponding transient mixing degree of the viscoelastic fluid.

the mixing channel width $W_2 = 600$ µm microchannel. This is due to a reduction in the mutual elastic stress between fluid A and fluid B in a wider "mixing channel" and the diffusion in the channel also decreases. Therefore, the transient mixing degree only remains around 40%. However, when the modulation frequency decreases to $f = 0.2$ Hz and $f = 0.1$ Hz, there is enough fluid A and fluid B interacting with each other in the bottleneck channel and forms a relatively high mixing region, so an obvious high mixing narrow band is formed in the mixing channel. For the most of the time, fluid A and fluid B are not well mixed when they enter the "mixing channel", and then gradually mix with each other due to the diffusion caused by the elastic interaction between them. The transient mixing degree therefore gradually increases as the fluid flows forward.

According to the previous analysis, the interaction between fluid A and fluid B in the bottleneck channel affects the mixing significantly. We investigated the length effect of the bottleneck channel by increasing it from 600 µm to 1400 µm as shown on the left side of **Figure 6B**. In this long bottleneck microchannel, the transient mixing degree of the PAM solution when $Q_0 = 500$ µL/h is shown on the right side of **Figure 6B**. The mixing degree fluctuation of the fluid in the long bottleneck microchannel is relatively small and the high mixing bands at different modulated frequencies are much less obvious compared to the cases when $L_2 = 600$ µm. This is because the interaction between fluid A and fluid B is constrained and stabilized in the long bottleneck channel.

As the interaction between fluid A and fluid B is constrained in the long bottleneck channel, we then propose a bent bottleneck channel, the side wall of which will exert an extra force on the fluids and therefore can increase the interaction between the fluids. The bent bottleneck microchannel is shown in **Figure 7A**. We compared the transient mixing of the PAM solution at the injection flow rate of 500 µL/h and 1000 µL/h as shown in **Figure 7B** and **7C**. Compared with the mixing in the long straight bottleneck microchannel, it is obvious that high mixing bands are induced in the bent bottleneck microchannel, which is caused by the enhanced interaction in the bent bottleneck channel. At the constant injection condition, the high mixing region appears at around $t = 4$ s and $t = 10$ s when entering the mixing channel. As the fluid flows forward, the high mixing bands expand significantly. This is different from the mixing in the straight bottleneck microchannel; for example, the fluids in **Figures 5** and **6** simply flow forward and the high mixing band does not expand much. The high mixing band in the bent bottleneck microchannel is even significant when the flow rate increases to 1000 µL/h. A higher centripetal force is induced at this higher flow rate condition; therefore, the mixing is increased and even the diffusion is affected at this high flow rate. At the driving frequency of $f = 1$ Hz, regular high mixing regions with the same period are observed when $Q_0 = 500$ µL/h. While for $Q_0 = 1000$ µL/h, the mixing is increased due to the stronger interaction between the fluids.

## Conclusions

In conclusion, the flow of the viscoelastic fluid in the microchannel structure is studied to mimic the blood flow in vessels. Specifically, two streams of PAM fluids are confronted

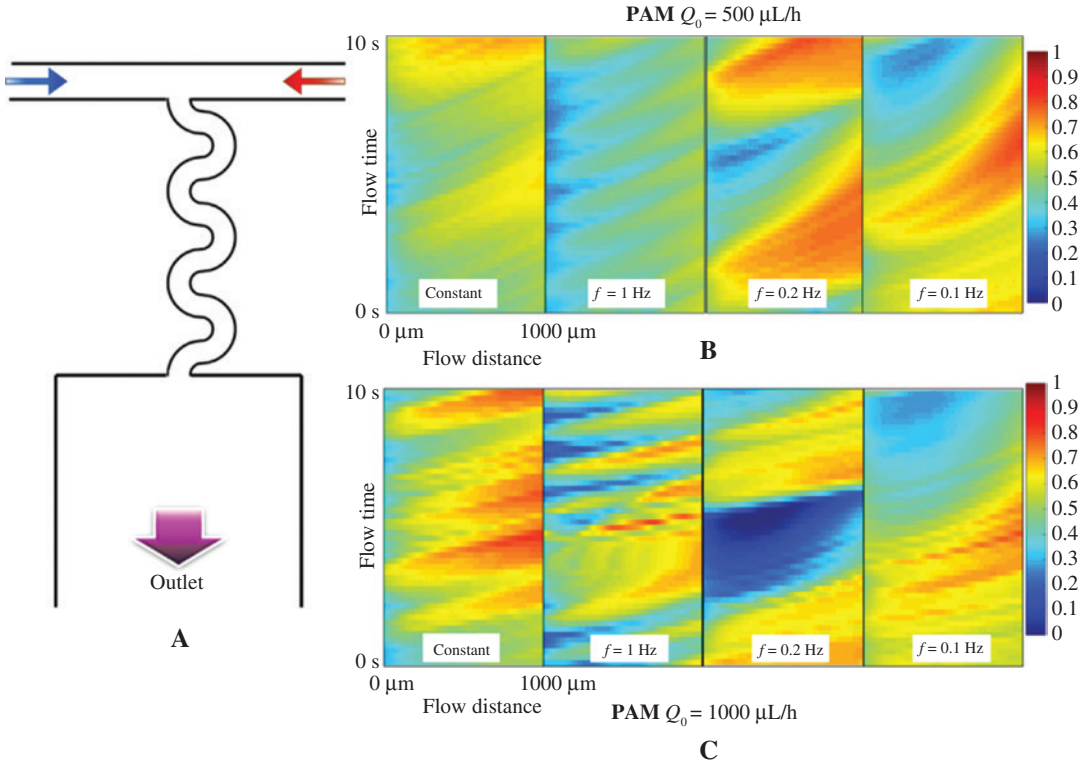


**Figure 7** (A) Schematic of an S-neck T-microchannel; (B) Mixing degree of the Newtonian fluid when $Q_0$ = 500 µL/h and (C) $Q_0$ = 1000 µL/h at different flow times and flow distances.

in a T-shaped microchannel, and the dye concentration profile and transient mixing between the two fluids are investigated. It demonstrates that the dye concentration profile in the viscoelastic flow changes with time even when the injection flow rate remains constant, which is due to the elastic interaction between the two streams. High transient mixing is observed periodically when the one side fluid is driven by periodical pulse stimulus. The approach to integrate microfluidic technology with the blood flow research will provide a new platform to understand the related biological mechanism, and the transient mixing degree of the flow can be used as a reference to investigate the blood flow in vessels.

## Acknowledgment

This work was supported by the National Natural Science Youth Foundation of China (No. 61905046).

## References

[1] Choi NW, Cabodi M, Held B, Gleghorn JP, Bonassar LJ, et al. Microfluidic scaffolds for tissue engineering. Nat Mater 2007;6:908-15. [PMID: 17906630 DOI: 10.1038/nmat2022]

[2] Cramer SM, Larson TS, Lockett MR. Tissue papers: leveraging paper-based microfluidics for the next generation of 3D tissue models. Anal Chem 2019;91:10916-26. [PMID: 31356054 DOI: 10.1021/acs.analchem.9b02102]

[3] Hoshino K, Huang Y-Y, Lane N, Huebschman M, Uhr JW, et al. Microchip-based immunomagnetic detection of circulating tumor cells. Lab Chip 2011;11:3449-57. [PMID: 21863182 DOI: 10.1039/C1LC20270G]

[4] Zuo P, Li X, Dominguez DC, Ye B-C. A PDMS/paper/glass hybrid microfluidic biochip integrated with aptamer-functionalized graphene oxide nano-biosensors for one-step multiplexed pathogen detection. Lab Chip 2013;13:3921-8. [PMID: 23929394 DOI: 10.1039/c3lc50654a]

[5] Vu HN, Li Y, Casali M, Irimia D, Megeed Z, et al. A microfluidic bioreactor for increased active retrovirus output. Lab Chip 2008;8:75-80. [PMID: 18094764 DOI: 10.1039/b711577f]

[6] Xu J, Zhang S, Machado A, Lecommandoux S, Sandre O, et al. Controllable microfluidic production of drug-loaded PLGA nanoparticles using partially water-miscible mixed solvent microdroplets as a precursor. Sci Rep 2017;7:4794. [PMID: 28684775 DOI: 10.1038/s41598-017-05184-5]

[7] Hong L, Dong Y-D, Boyd BJ. Preparation of nanostructured lipid drug delivery particles using microfluidic mixing. Pharm Nanotechnol 2019;7:484-95. [PMID: 31584384 DOI: 10.2174/2211738507666191004123545]

[8] Cai S, Shi H, Li G, Xue Q, Zhao L, et al. 3D-printed concentration-controlled microfluidic chip with diffusion mixing pattern for the synthesis of alginate drug delivery microgels. Nanomaterials 2019;9:1451. [PMID: 31614763 DOI: 10.3390/nano9101451]

[9] Leung AKK, Hafez IM, Baoukina S, Belliveau NM, Zhigaltsev IV, et al. Lipid nanoparticles containing siRNA synthesized by microfluidic mixing exhibit an electron-dense nanostructured core. J Phys Chem C 2012;116:18440-50. [PMID: 22962627 DOI: 10.1021/jp303267y]

[10] Duguay BA, Huang KW-C, Kulka M. Lipofection of plasmid DNA into human mast cell lines using lipid nanoparticles generated by microfluidic mixing. J Leukoc Biol 2018;104:587-96. [PMID: 29668121 DOI: 10.1002/JLB.3TA0517-192R]

[11] Verma S, Panda S. Effect of active mixing on capture efficiency in heterogeneous microfluidic immunosensor. Microfluid Nanofluid 2020;24:58. [DOI: 10.1007/s10404-020-02364-0]

[12] Guo J, Zhang R, Yang N, Xu P. Electric field control chaotic mixing method for immunoagglutination microfluidic detection system. Chinese J Sci Instrum 2014;35:685-90.

[13] Imran JH, Kim JK. A nut-and-bolt microfluidic mixing system for the rapid labeling of immune cells with antibodies. Micromachines 2020;11:280. [PMID: 32182878 DOI: 10.3390/mi11030280]

[14] Natsuhara D, Takishita K, Tanaka K, Kage A, Suzuki R, et al. A microfluidic diagnostic device capable of autonomous sample mixing and dispensing for the simultaneous genetic detection of multiple plant viruses. Micromachines 2020;11:540. [PMID: 32466570 DOI: 10.3390/mi11060540]

[15] Yoon HK, Lou X, Chen Y-C, Lee Y-EK, Yoon E, et al. Nanophotosensitizers engineered to generate a tunable mix of reactive oxygen species, for optimizing photodynamic therapy, using a microfluidic device. Chem Mater 2014;26:1592-600. [PMID: 24701030 DOI: 10.1021/cm403505s]

[16] Morikawa Y, Tagami T, Hoshikawa A, Ozeki T. The use of an efficient microfluidic mixing system for generating stabilized polymeric nanoparticles for controlled drug release. Biol Pharm Bull 2018;41:899-907. [PMID: 29863078 DOI: 10.1248/bpb.b17-01036]

[17] Wu J, Tomsa D, Zhang M, Komenda P, Tangri N, et al. A passive mixing microfluidic urinary albumin chip for chronic kidney disease assessment. ACS Sens 2018;3:2191-7. [PMID: 30350581 DOI: 10.1021/acssensors.8b01072]

[18] Anastasiou AD, Spyrogianni AS, Koskinas KC, Giannoglou GD, Paras SV. Experimental investigation of the flow of a blood analogue fluid in a replica of a bifurcated small artery. Med Eng Phys 2012;34:211-8. [PMID: 21824798 DOI: 10.1016/j.medengphy.2011.07.012]

[19] Boyd J, Buick J, Cosgrove JA, Stansell P. Application of the lattice Boltzmann model to simulated stenosis growth in a two-dimensional carotid artery. Phys Med Biol 2005;50:4783-96. [PMID: 16204872 DOI: 10.1088/0031-9155/50/20/003]

[20] Yap C-H, Dasi LP, Yoganathan AP. Dynamic hemodynamic energy loss in normal and stenosed aortic valves. J Biomech Eng-Transactions ASME 2010;132. [PMID: 20370242 DOI: 10.1115/1.4000874]

[21] Karri S, Vlachos PP. Time-resolved DPIV investigation of pulsatile flow in symmetric stenotic arteries effects of phase angle. J Biomech Eng-Transactions ASME 2010;132. [PMID: 20459198 DOI: 10.1115/1.4000934]

[22] Chakravarty S, Mandal PK. Two-dimensional blood flow through tapered arteries under stenotic conditions. Int J NonLin Mech 2000;35:779-93. [DOI: 10.1016/S0020-7462(99)00059-1]

[23] Riahi DN, Roy R, Cavazos S. On arterial blood flow in the presence of an overlapping stenosis. Math Comput Model 2011;54:2999-3006. [DOI: 10.1016/j.mcm.2011.07.028]

[24] Ikbal MA, Chakravarty S, Sarifuddin, Mandal PK. Unsteady analysis of viscoelastic blood flow through arterial stenosis. Chem Eng Commun 2012;199 40-62. [DOI: 10.1080/00986445.2011.569802]

[25] Anguiano M, Castilla C, Maska M, Ederra C, Pelaez R, et al. Characterization of three-dimensional cancer cell migration in mixed collagen-Matrigel scaffolds using microfluidics and image analysis. PLoS One 2017;12:e0171417. [PMID: 28166248 DOI: 10.1371/journal.pone.0171417]

[26] Novo P, Volpetti F, Chu V, Conde JP. Control of sequential fluid delivery in a fully autonomous capillary microfluidic device. Lab Chip 2013;13:641-5. [PMID: 23263650 DOI: 10.1039/c2lc41083d]

[27] Lapizco-Encinas BH. On the recent developments of insulator-based dielectrophoresis: a review. Electrophoresis 2019;40:358-75. [PMID: 30112789 DOI: 10.1002/elps.201800285]

[28] Chen C, Skog J, Hsu C-H, Lessard RT, Balaj L, et al. Microfluidic isolation and transcriptome analysis of serum microvesicles. Lab Chip 2010;10:505-11. [PMID: 20126692 DOI: 10.1039/b916199f]

[29] Joensson HN, Samuels ML, Brouzes ER, Medkova M, Uhlen M, et al. Detection and analysis of low-abundance cell-surface

biomarkers using enzymatic amplification in microfluidic droplets. Angew Chem Int Ed 2009;48:2518-21. [PMID: 19235824 DOI: 10.1002/anie.200804326]

[30] Wang S, Zhang X, Yu B, Lee RJ, Lee LJ. Targeted nanoparticles enhanced flow electroporation of antisense oligonucleotides in leukemia cells. Biosens Bioelectron 2010;26:778-83. [PMID: 20630739 DOI: 10.1016/j.bios.2010.06.025]

[31] Wang J, Zhan Y, Ugaz VM, Lu C. Vortex-assisted DNA delivery. Lab Chip 2010;10:2057-61. [PMID: 20563345 DOI: 10.1039/c004472e]

[32] Kuramoto H, Park Y-S, Kaji N, Tokeshi M, Kogure K, et al. On-chip fabrication of mutifunctional envelope-type nanodevices for gene delivery. Anal Bioanal Chem 2008;391:2729-33. [PMID: 18542934 DOI: 10.1007/s00216-008-2124-7]

[33] Zhang M, Zhang W, Wu Z, Shen Y, Chen Y, et al. Comparison of micro-mixing in time pulsed Newtonian fluid and viscoelastic fluid. Micromachines 2019;10:262. [PMID: 31003548 DOI: 10.3390/mi10040262]

[34] Park Y-M, Hong SO, Lee PC, Kim JM. Vortex dynamics at the junction of Y-shaped microchannels in dilute polymer solutions. Korea-Aust Rheol J 2019;31:189-94. [DOI: 10.1007/s13367-019-0019-0]

[35] Kim DY, Kim JM. Vortex generation by viscoelastic sheath flow in flow-focusing microchannel. Korean J Chem Eng 2019;36:837-42. [DOI: 10.1007/s11814-019-0272-4]

[36] Hong SO, Cooper-White JJ, Kim JM. Inertio-elastic mixing in a straight microchannel with side wells. Appl Phys Lett 2016;108:014103. [DOI: 10.1063/1.4939552]

[37] Gijsen FJH, Allanic E, van de Vosse FN, Janssen JD. The influence of the non-Newtonian properties of blood on the flow in large arteries: unsteady flow in a 90 degrees curved tube. J Biomech 1999;32:705-13. [PMID: 10400358 DOI: 10.1016/S0021-9290(99)00014-7]

[38] Sousa PC, Pinho FT, Oliveira MSN, Alves MA. Extensional flow of blood analog solutions in microfluidic devices. Biomicrofluidics 2011;5:14108. [PMID: 21483662 DOI: 10.1063/1.3567888]

[39] Ji HS, Lee SJ. In vitro hemorheological study on the hematocrit effect of human blood flow in a microtube. Clin Hemorheol Micro 2008;40:19-30. [PMID: 18791264 DOI: 10.3233/CH-2008-1059]

[40] Saengow C, Giacomin AJ, Dimitrov AS. Unidirectional large-amplitude oscillatory shear flow of human blood. Phys Fluids 2019;31:111903. [DOI: 10.1063/1.5127868]